Scientific Research Publishing

Open Journal of Applied Sciences, 2022, 12, 1352-1365
https://www.scirp.org/journal/ojapps
ISSN Online: 2165-3925
ISSN Print: 2165-3917

Dynamic Analysis of Nanosized Arbitrary Shape Inclusion under SH Waves

Yongqiang Sun

Department of Basic Education Research, Xinjiang University of Science and Technology, Kuerle, China
Email: 15009313419@163.com

How to cite this paper: Sun, Y.Q. (2022) Dynamic Analysis of Nanosized Arbitrary Shape Inclusion under SH Waves. *Open Journal of Applied Sciences*, **12**, 1352-1365.
https://doi.org/10.4236/ojapps.2022.128093

Received: July 13, 2022
Accepted: August 15, 2022
Published: August 18, 2022

Abstract

The scattering of shear waves (SH waves) by nano-scale arbitrary shape inclusion in infinite plane is studied by complex variable function theory. Firstly, the governing equation and the relationships between stress and displacement are given by classical elastic theory. Secondly, the arbitrary shape inclusion in the two-dimensional plane is transformed into a unit circle domain by conformal mapping, the incident wave field and the scattered wave field are presented. Next, the stress and displacement boundary conditions are established by considering surface elasticity theory, The infinite algebraic equations for solving the unknown coefficients of the scattered and standing waves are obtained. Finally, the influence of surface effect, non-dimensional wave number, Shear modulus and hole curvature on the dynamic stress concentration factor are analyzed by some examples, the numerical results show that the surface effect weakens the dynamic stress concentration. With the increase of wave number, the dynamic stress concentration factor (DSCF) decreases. Shear modulus and hole curvature have significant effects on DSCF.

Keywords

SH Waves, Arbitrary Shape Inclusion, Conformal Transformation, Surface Effect, Dynamic Stress Concentration Factor

1. Introduction

Wave propagation in different kinds of media attracts lots of attentions in many fields for decades. Since different media or defects (cavities, inclusions, or cracks), which influence the stresses in continuous media or structures, usually exist in practical engineering, dynamic response of complex medium with defects and inclusions embedded under elastic waves should be considered seriously. Clebsch opened a precedent for the study of elastic wave scattering by

studying the scattering effect of spherical inclusions on elastic waves. Baron and Mattews used integral transformation and wave function expansion to study the pulse compression wave scattering problem caused by cylindrical holes in elastic media, and gave an analytical solution to the problem [1]. Reference [2] discussed the scattering of elliptical cylinders by using the wave function expansion method. Reference [3] investigated the problem of SH-wave scattering and dynamic stress concentration by bi-material structure possessing cylindrical interface hole and discussed the effect of the combination of different medium parameters on the dynamic stress concentration. Reference [4] studied the scattering problem of circular holes in half space. Reference [5] researched the scattering and dynamic stress concentration of SH-wave by removable rigid cylindrical interface inclusion by presenting the development of a suitable green's function. Reference [6] studied Scattering of SH wave and ground motion in an elastic half space containing an elastic cylindrical inclusion and a crack located at any position and direction by using Green's function, complex function and multi-polar coordinate system. Numerical examples are used to discuss the effects of various parameters on the surface displacement above the inclusions. Reference [7] studied the dynamic response of anisotropic elastic half-space containing cylindrical holes under the action of steady-state horizontal shear (SH) waves, and discussed the influence of the anisotropy of the medium on the dynamic stress near the hole. Reference [8] investigates scattering of elastic waves around a homogeneous circular inclusion buried in a radially inhomogeneous elastic medium by using the complex function theory.

However, in the aforementioned studies, the effect of the interface stress was not taken into account. The influence of inclusions with surface energy on the mechanical behavior of inhomogeneous nanomaterials has been extensively studied with the Gurtin-Murdoch model [9]. Reference [10] [11] analyzed the significance of surface effect on the size-dependent behavior of nanostructured components. Reference [12] considered the diffraction of P-wave by a nanosized circular hole, the surface elasticity theory is employed to incorporate the surface effects, the results show that once the radius of hole reduces to nanometers, surface energy significantly affects the diffraction of elastic waves. Reference [13] investigated the multiple diffraction of plane harmonic compressional waves by two nanosized circular cylindrical holes embedded in an elastic solid. The surface elasticity theory is adopted to account for the effect of surface energy at nanoscales. Reference [14] described the diffraction of elastic waves and the stress concentration near a cylindrical nano-inclusion with surface effect by using the displacement potential method. Reference [15] studied the scattering of plane compressional and shear waves by a single nano-sized coated fiber embedded in an elastic matrix using the method of eigenfunction expansion. The dynamic stress concentration factors along the interface between the coated fiber and the matrix induced by the plane elastic wave and scattering cross section are derived and numerically evaluated. Reference [16] investigated the multiple scattering of

plane compressional waves by two cylindrical fibers with interface effects. Based on surface elasticity theory, the wave fields in a nanoscale solid medium be obtained by applying the eigenfunction expansion method and the Graf's addition theorem. Reference [17] described surface effects on the scatter of SH-Wave by a shallow buried the elliptical hole. The surface elasticity theory is applied to obtain the stress boundary conditions on the surface.

This paper aims to research the scattering of shear waves by nano-scale arbitrary shape inclusion in infinite plan. Based on the conformal mapping method, incident waves, scattering waves and standing waves are obtained. Considering different parameters, dynamic stress concentration around the arbitrary shape inclusion is calculated and discussed. The validity of the method is confirmed, and the influential factors of dynamic stress concentration factor are determined.

2. Description of the Problem

Scattering model of an arbitrary shape inclusion under SH wave with incident angle α is shown in **Figure 1**. The medium I and the arbitrary shape inclusion (medium II) are homogeneous and isotropic. The boundary of the arbitrary shape inclusion is *S*, and the origin of the polar coordinate system coincides with the center of the inclusion.

Under antiplane shear wave (SH waves) model, supposing harmonic response and supposing that the body force equals to zero, the governing equation in Cartesian coordinate can be expressed as [7]

$$\nabla^2 W + k^2 W = 0 \tag{1}$$

where $W = W(x, y)$ is the displacement function and $k = \omega/c$ is the wave number. ω is the circular frequency of the displacement W, $c = \sqrt{\mu/\rho}$ is the velocity of shear wave, ρ and μ are the mass density and the shear modulus.

Due to that the medium is isotropic, the constitutive relations between stresses and displacements can be expressed as

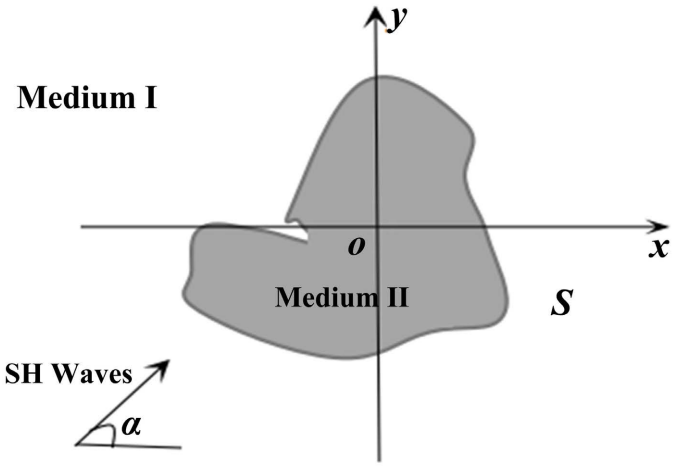

Figure 1. The scattering model.

$$\sigma_{xz} = \mu \frac{\partial W}{\partial x}, \quad \sigma_{yz} = \mu \frac{\partial W}{\partial y} \tag{2}$$

Based on complex function method, a pair of complex variables are introduced

$$z = x + \mathrm{i}y, \ \overline{z} = x - \mathrm{i}y \tag{3}$$

then, the Equation (1) and Equation (2) in complex coordinates are obtained

$$\frac{\partial^2 W}{\partial z \partial \overline{z}} + \frac{1}{4} k^2 W = 0 \tag{4}$$

$$\sigma_{xz} = \mu \left(\frac{\partial W}{\partial z} + \frac{\partial W}{\partial \overline{z}} \right), \quad \sigma_{yz} = \mathrm{i}\mu \left(\frac{\partial W}{\partial z} - \frac{\partial W}{\partial \overline{z}} \right) \tag{5}$$

The relations between stresses and displacements in polar coordinate can be written as

$$\tau_{rz} = \mu \left(\frac{\partial W}{\partial z} \mathrm{e}^{\mathrm{i}\theta} + \frac{\partial W}{\partial \overline{z}} \mathrm{e}^{-\mathrm{i}\theta} \right), \ \tau_{\theta z} = \mathrm{i}\mu \left(\frac{\partial W}{\partial z} \mathrm{e}^{\mathrm{i}\theta} - \frac{\partial W}{\partial \overline{z}} \mathrm{e}^{-\mathrm{i}\theta} \right) \tag{6}$$

The irregular boundary can be transformed into the unit-circle boundary in the mapping plane by the conformal mapping. The outer domain of the irregular boundary corresponds to the outer domain of the unit circle in the mapping plane. Introducing conformal mapping $z = \omega(\eta)$ is shown in Figure 2.

According to the transition relation between the arbitrary shape inclusion and the unit circle, it yields

$$\mathrm{e}^{\mathrm{i}\theta} = \frac{\eta \omega'(\eta)}{\left|\omega'(\eta)\right|}, \ \mathrm{e}^{-\mathrm{i}\theta} = \frac{\overline{\eta \omega'(\eta)}}{\left|\omega'(\eta)\right|} \tag{7}$$

Substituting conformal mapping $z = \omega(\eta)$ into Equation (4), the following equation in the η plane is obtained

$$\frac{1}{\omega'(\eta)\overline{\omega'(\eta)}} \frac{\partial^2 W}{\partial \eta \partial \overline{\eta}} + \frac{1}{4} k^2 W = 0 \tag{8}$$

According to Equation (6) and Equation (7), the relations between stresses and displacements in the η plane can be written as

$$\sigma_{rz} = \frac{\mu}{\left|\omega'(\eta)\right|} \left(\frac{\partial W}{\partial \eta} \eta + \frac{\partial W}{\partial \overline{\eta}} \overline{\eta} \right), \ \sigma_{\theta z} = \frac{\mathrm{i}\mu}{\left|\omega'(\eta)\right|} \left(\frac{\partial W}{\partial \eta} \eta - \frac{\partial W}{\partial \overline{\eta}} \overline{\eta} \right) \tag{9}$$

Based on the derivation in the section above, the incident waves which propagates with α in medium I can be expressed as

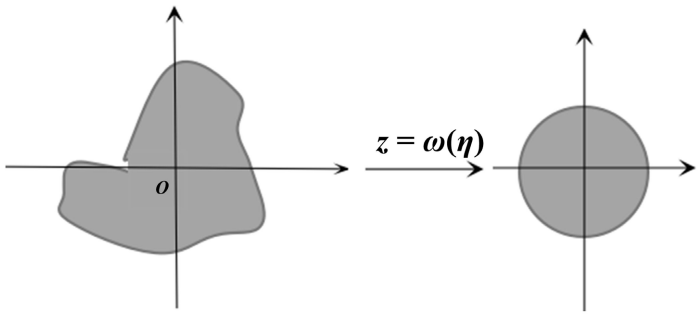

Figure 2. Conformal mapping process of a non-circular inclusion.

$$W^{(\mathrm{Inc})} = W_0 \exp\left[\frac{\mathrm{i}k_1}{2}\left(\omega(\eta)\mathrm{e}^{-\mathrm{i}\alpha} + \overline{\omega(\eta)}\mathrm{e}^{\mathrm{i}\alpha}\right)\right] \tag{10}$$

where W_0 is the displacement amplitude of incident waves, and k_1 is the wave number of the medium I.

According to Equation (8), the scattering waves excited by the arbitrary shape inclusion obeys

$$W^{(\mathrm{Sca})} = \sum_{n=-\infty}^{+\infty} A_n H_n^{(1)}\left(k_1\left|\omega(\eta)\right|\right)\left(\frac{\omega(\eta)}{\left|\omega(\eta)\right|}\right)^n \tag{11}$$

where A_n are undetermined coefficients and $H_n^{(1)}(\cdot)$ is the first kind Hankel function of the nth order.

The standing waves in medium II can be expressed as

$$W^{(\mathrm{Sta})} = \sum_{n=-\infty}^{+\infty} B_n J_n\left(k_2\left|\omega(\eta)\right|\right)\left(\frac{\omega(\eta)}{\left|\omega(\eta)\right|}\right)^n \tag{12}$$

where B_n are undetermined coefficients, $J_n(\cdot)$ is the Bessel function of the nth order, and k_2 is the wave number corresponding to medium II.

Substituting different displacement fields into Equation (9), respectively, the detailed stress components can be obtained.

$$\sigma_{rz}^{(\mathrm{Inc})} = \frac{\mathrm{i}k_1\mu_1}{2}\exp\left\{\frac{\mathrm{i}k_1}{2}\left[\omega(\eta)\mathrm{e}^{-\mathrm{i}\alpha} + \overline{\omega(\eta)}\mathrm{e}^{\mathrm{i}\alpha}\right]\right\}\left[\frac{\eta\omega'(\eta)}{\left|\omega'(\eta)\right|}\mathrm{e}^{-\mathrm{i}\alpha} + \frac{\overline{\eta\omega'(\eta)}}{\left|\omega'(\eta)\right|}\mathrm{e}^{\mathrm{i}\alpha}\right] \tag{13}$$

$$\sigma_{\theta z}^{(\mathrm{Inc})} = -\frac{k_1\mu_1}{2}\exp\left\{\frac{\mathrm{i}k_1}{2}\left[\omega(\eta)\mathrm{e}^{-\mathrm{i}\alpha} + \overline{\omega(\eta)}\mathrm{e}^{\mathrm{i}\alpha}\right]\right\}\left[\frac{\eta\omega'(\eta)}{\left|\omega'(\eta)\right|}\mathrm{e}^{-\mathrm{i}\alpha} - \frac{\overline{\eta\omega'(\eta)}}{\left|\omega'(\eta)\right|}\mathrm{e}^{\mathrm{i}\alpha}\right] \tag{14}$$

$$\begin{aligned}\sigma_{rz}^{(\mathrm{Sca})} = \frac{k_1\mu_1}{2}\sum_{n=-\infty}^{+\infty} A_n\Bigg\{&H_{n-1}^{(1)}\left[k_1\left|\omega(\eta)\right|\right]\left[\frac{\omega(\eta)}{\left|\omega(\eta)\right|}\right]^{n-1}\frac{\eta\omega'(\eta)}{\left|\omega'(\eta)\right|}\\ &- H_{n+1}^{(1)}\left[k_1\left|\omega(\eta)\right|\right]\left[\frac{\omega(\eta)}{\left|\omega(\eta)\right|}\right]^{n+1}\frac{\eta\omega'(\eta)}{\left|\omega'(\eta)\right|}\Bigg\}\end{aligned} \tag{15}$$

$$\begin{aligned}\sigma_{\theta z}^{(\mathrm{Sca})} = \frac{\mathrm{i}k_1\mu_1}{2}\sum_{n=-\infty}^{+\infty} A_n\Bigg\{&H_{n-1}^{(1)}\left[k_1\left|\omega(\eta)\right|\right]\left[\frac{\omega(\eta)}{\left|\omega(\eta)\right|}\right]^{n-1}\frac{\eta\omega'(\eta)}{\left|\omega'(\eta)\right|}\\ &+ H_{n+1}^{(1)}\left[k_1\left|\omega(\eta)\right|\right]\left[\frac{\omega(\eta)}{\left|\omega(\eta)\right|}\right]^{n+1}\frac{\eta\omega'(\eta)}{\left|\omega'(\eta)\right|}\Bigg\}\end{aligned} \tag{16}$$

$$\begin{aligned}\sigma_{rz}^{(\mathrm{Sta})} = \frac{k_2\mu_2}{2}\sum_{n=-\infty}^{+\infty} B_n\Bigg\{&J_{n-1}\left[k_2\left|\omega(\eta)\right|\right]\left[\frac{\omega(\eta)}{\left|\omega(\eta)\right|}\right]^{n-1}\frac{\eta\omega'(\eta)}{\left|\omega'(\eta)\right|}\\ &- J_{n+1}\left[k_2\left|\omega(\eta)\right|\right]\left[\frac{\omega(\eta)}{\left|\omega(\eta)\right|}\right]^{n+1}\frac{\eta\omega'(\eta)}{\left|\omega'(\eta)\right|}\Bigg\}\end{aligned} \tag{17}$$

$$\sigma_{\theta z}^{(\mathrm{Sta})}=\frac{\mathrm{i}k_2\mu_2}{2}\sum_{n=-\infty}^{+\infty}B_n\left\{J_{n-1}\left[k_2\left|\omega(\eta)\right|\right]\left[\frac{\omega(\eta)}{\left|\omega(\eta)\right|}\right]^{n-1}\frac{\eta\omega'(\eta)}{\left|\omega'(\eta)\right|}\right.$$
$$\left.+J_{n+1}\left[k_2\left|\omega(\eta)\right|\right]\left[\frac{\omega(\eta)}{\left|\omega(\eta)\right|}\right]^{n+1}\frac{\eta\omega'(\eta)}{\left|\omega'(\eta)\right|}\right\} \tag{18}$$

where k_1 is the wave number of the medium I, k_2 is the wave number corresponding to medium II. μ_1 and μ_2 are the equivalent shear modulus of the medium I and medium II, respectively.

At the interface of the arbitrary shape inclusion, the boundary condition is the continuity condition of the wave fields and the radial shear stresses

$$W_{\mathrm{I}}=W_{\mathrm{II}} \tag{19}$$

$$\sigma_{rz,\mathrm{I}}=\sigma_{rz,\mathrm{II}} \tag{20}$$

where $W_{\mathrm{I}}=W^{(\mathrm{Inc})}+W^{(\mathrm{Sca})}$, $W_{\mathrm{II}}=W^{(\mathrm{Sta})}$, $\sigma_{rz,\mathrm{I}}=\sigma_{rz}^{(\mathrm{Inc})}+\sigma_{rz}^{(\mathrm{Sca})}$, $\sigma_{rz,\mathrm{II}}=\sigma_{rz}^{(\mathrm{Sta})}$.

3. Surface Elasticity and the Resulting Boundary Conditions

To incorporate the surface/interface effect into this study, the Gurtin-Murdoch surface elastic model was used in this paper. The interface is regarded as negligibly thin membranes that adhere to the bulk without slipping and it has material constants different from those of the bulk. The equilibrium equations on the interface can be expressed as [12]

$$\left(\tau-\tau^{1}\right)\boldsymbol{n}=-\nabla_s\cdot\tau^{s} \tag{21}$$

where τ, τ^{1} and τ^{s} are stresses of the medium I, medium II and interface respectively. $\boldsymbol{n}$ is the normal vector of the surface. $\nabla_s\cdot\tau^{s}$ is the divergence of the surface.

The constitutive equation of the surface can be written as

$$\sigma_{\alpha\beta}^{s}=\tau^{0}\delta_{\alpha\beta}+2\left(\mu^{s}-\tau^{0}\right)\delta_{\alpha\gamma}\varepsilon_{\gamma\beta}+\left(\lambda^{s}+\tau^{0}\right)\varepsilon_{\gamma\gamma}\delta_{\alpha\beta} \tag{22}$$

where τ^{0} denotes the residual tension of the surface. μ^{s} and λ^{s} are the surface parameters. $\tau_{\alpha\beta}^{s}$ denotes the stress of the surface. $\delta_{\alpha\beta}$ is the Kronecker delta.

According to Equation (22), the stress of the surface $\tau_{\theta z}^{s}$ is obtained

$$\tau_{\theta z}^{s}=2\mu^{s}\varepsilon_{\theta z} \tag{23}$$

According to the equilibrium equation in the medium I, the total stress $\tau_{\theta z}$ can be expressed as

$$\tau_{\theta z}=2\mu\varepsilon_{\theta z} \tag{24}$$

Substituting Equation (24) to Equation (23), the stress of the surface $\tau_{\theta z}^{s}$ can be written as

$$\tau_{\theta z}^{s}=\frac{\mu^{s}}{\mu}\tau_{\theta z} \tag{25}$$

For a circular hole with radius $r=a$, according to Equation (21), we find

$$\tau_{rz} = -\frac{1}{a}\frac{\partial \tau_{\theta z}^{s}}{\partial \theta} \tag{26}$$

Substituting Equation (25) to Equation (26), the stress boundary conditions around the circular hole can be obtained

$$\tau_{rz} = -s\frac{\partial \tau_{\theta z}}{\partial \theta} \tag{27}$$

where $s = \mu^{s}/a\mu$ is a dimensionless parameter that reflects the effect of the surface/interface on the nanoscale. It decreases with the increase of radius, which objectively reflects the fact that the surface effect not be considered for macroscopic objects, but the size of the object is very small, the surface effect is too significant to ignore.

According to the Equation (19), Equation (20) and Equation (27), the boundary conditions of the arbitrary shape inclusion can be obtained

$$\begin{cases} W_{\mathrm{I}} = W_{\mathrm{II}} \\ \sigma_{rz,\mathrm{I}} - \sigma_{rz,\mathrm{II}} = -s\dfrac{\partial \sigma_{\theta z,\mathrm{I}}}{\partial \theta} \end{cases} \tag{28}$$

where $\sigma_{\theta z,\mathrm{I}} = \sigma_{\theta z}^{(\mathrm{Inc})} + \sigma_{\theta z}^{(\mathrm{Sca})}$. Hence, the boundary condition can be expressed as

$$\begin{cases} \sum\limits_{n=-\infty}^{+\infty}\left(A_n\varepsilon_n + B_n\delta_n\right) = \varepsilon \\ \sum\limits_{n=-\infty}^{+\infty}\left(A_n\xi_n + B_n\zeta_n\right) = \xi \end{cases} \tag{29}$$

where

$$\begin{gathered} \varepsilon_n = H_n^{(1)}\left(k_1\left|\omega(\eta)\right|\right)\left[\frac{\omega(\eta)}{\left|\omega(\eta)\right|}\right]^n,\ \delta_n = -J_n\left(k_2\left|\omega(\eta)\right|\right)\left[\frac{\omega(\eta)}{\left|\omega(\eta)\right|}\right]^n, \\ \varepsilon = -\exp\left\{\frac{\mathrm{i}k_1}{2}\left[\omega(\eta)\mathrm{e}^{-\mathrm{i}\alpha} + \overline{\omega(\eta)}\mathrm{e}^{\mathrm{i}\alpha}\right]\right\} \end{gathered} \tag{30}$$

$$\begin{aligned} \xi = {} & \frac{\mathrm{i}k_1\mu_1 s}{2}\exp\left\{\frac{\mathrm{i}k_1}{2}\left[\omega(\eta)\mathrm{e}^{-\mathrm{i}\alpha} + \overline{\omega(\eta)}\mathrm{e}^{\mathrm{i}\alpha}\right]\right\}\phi(\eta) \\ & + \frac{\mathrm{i}k_1\mu_1 s}{2}\exp\left\{\frac{\mathrm{i}k_1}{2}\left[\omega(\eta)\mathrm{e}^{-\mathrm{i}\alpha} + \overline{\omega(\eta)}\mathrm{e}^{\mathrm{i}\alpha}\right]\right\}\psi(\eta) \\ & + sk_1^{\,2}\mu_1\exp\left\{\frac{\mathrm{i}k_1}{2}\left[\omega(\eta)\mathrm{e}^{-\mathrm{i}\alpha} + \overline{\omega(\eta)}\mathrm{e}^{\mathrm{i}\alpha}\right]\right\}f(\eta) \\ & - \mathrm{i}k_1\mu_1\exp\left\{\frac{\mathrm{i}k_1}{2}\left[\omega(\eta)\mathrm{e}^{-\mathrm{i}\alpha} + \overline{\omega(\eta)}\mathrm{e}^{\mathrm{i}\alpha}\right]\right\}g(\eta) \end{aligned} \tag{31}$$

$$\begin{aligned} \zeta_n = {} & \frac{k_2\mu_2}{2}\left\{J_{n-1}\left[k_2\left|\omega(\eta)\right|\right]\left[\frac{\omega(\eta)}{\left|\omega(\eta)\right|}\right]^{n-1}\frac{\eta\omega'(\eta)}{\left|\omega'(\eta)\right|}\right. \\ & \left. + J_{n+1}\left[k_2\left|\omega(\eta)\right|\right]\left[\frac{\omega(\eta)}{\left|\omega(\eta)\right|}\right]^{n+1}\frac{\eta\omega'(\eta)}{\left|\omega'(\eta)\right|}\right\} \end{aligned} \tag{32}$$

$$\begin{aligned}\xi_n = &-\frac{sk_1^2\mu_1}{4}\left\{H_{n-2}^{(1)}\left[k_1|\omega(\eta)|\right]\left[\frac{\omega(\eta)}{|\omega(\eta)|}\right]^{n-2}\frac{\eta^2\left[\omega(\eta)\right]^2}{|\omega'(\eta)|}\right.\\ &\left.+H_{n-2}^{(1)}\left[k_1|\omega(\eta)|\right]\left[\frac{\omega(\eta)}{|\omega(\eta)|}\right]^{n-2}\frac{\overline{\eta}^2\left[\overline{\omega(\eta)}\right]^2}{|\omega'(\eta)|}+h(\eta)\right\}\\ &+\frac{k_1\mu_1}{2}\left\{H_{n-1}^{(1)}\left[k_1|\omega(\eta)|\right]\left[\frac{\omega(\eta)}{|\omega(\eta)|}\right]^{n-1}\left[\frac{\eta\omega'(\eta)}{|\omega'(\eta)|}-s\varphi(\eta)\right]\right.\\ &\left.+H_{n+1}^{(1)}\left[k_1|\omega(\eta)|\right]\left[\frac{\omega(\eta)}{|\omega(\eta)|}\right]^{n+1}\left[s\psi(\eta)-\frac{\overline{\eta}\,\overline{\omega'(\eta)}}{|\omega'(\eta)|}\right]\right\}\end{aligned} \tag{33}$$

where

$$h(\eta)=2H_n^{(1)}\left[k_1|\omega(\eta)|\right]\left[\frac{\omega(\eta)}{|\omega(\eta)|}\right]^n|\omega'(\eta)|,\quad f(\eta)=\frac{\left\{\mathrm{Im}\left[\omega'(\eta)\eta e^{-i\alpha}\right]\right\}^2}{|\omega'(\eta)|} \tag{34}$$

$$g(\eta)=\frac{\mathrm{Re}\left[\omega'(\eta)\eta e^{-i\alpha}\right]}{|\omega'(\eta)|}$$

$$\varphi(\eta)=\frac{\eta\omega'(\eta)+\eta^2\omega''(\eta)}{|\omega'(\eta)|}-\frac{\eta\omega'(\eta)\mathrm{Re}\left[\omega''(\eta)\eta\overline{\omega'(\eta)}\right]}{2|\omega'(\eta)|^3} \tag{35}$$

$$\psi(\eta)=\frac{\overline{\eta}\,\overline{\omega'(\eta)}+\overline{\eta}^2\overline{\omega''(\eta)}}{|\omega'(\eta)|}+\frac{\overline{\eta}\,\overline{\omega'(\eta)}\mathrm{Re}\left[\omega''(\eta)\eta\overline{\omega'(\eta)}\right]}{2|\omega'(\eta)|^3} \tag{36}$$

Multiplying $e^{-im\theta}$ with both sides of Equation (29) and integrating on the interval $(-\pi,\pi)$ yields

$$\sum_{n=-\infty}^{+\infty}\begin{bmatrix}\varepsilon_{mn} & \delta_{mn}\\ \xi_{mn} & \zeta_{mn}\end{bmatrix}\begin{bmatrix}A_n\\ B_n\end{bmatrix}=\begin{bmatrix}\varepsilon_m\\ \xi_m\end{bmatrix}\quad\begin{cases}m=0,\pm1,\pm2\cdots\\ n=0,\pm1,\pm2\cdots\end{cases} \tag{37}$$

hence, a set of infinite algebraic equation for unknown constants A_n will be obtained from Equation (37).

4. Numerical Results and Discussion

Based on the definition of dynamic stress concentration factor (DSCF), the expression of DSCF can be expressed as

$$\sigma_{\mathrm{DSCF}}=\left|\frac{\sigma_{\theta z,\mathrm{I}}}{\sigma_0}\right| \tag{38}$$

where $\sigma_0=\frac{1}{2}\mu_1k_1W_0$ is the stress amplitude of incident wave.

In order to validate the present approach, a degenerated result is considered to compare with published result. In **Figure 3**, we set $k_2=0$, $\mu_2=0$, $z=\omega(\eta)=a\eta$ to simulate the condition of plane SH wave propagating in medium with a circular cavity. The numerical results coincide with the results by

Pao and Mow perfectly [2].

Introducing conformal mapping $z = R(\eta + m/\eta)$, where $R = (a+b)/2$, $m = (a-b)/(a+b)$. We set the wave number ratio $k^* = k_1/k_2$, shear modulus ratio $\mu^* = \mu_1/\mu_2$ and the ratio of long semi-axis and short semi-axis $m^* = b/a$. **Figure 4** shows the distribution of DSCF at surface parameter $s = 0, 0.1, 0.5, 1$ when k^*, μ^*, m^* equal 0.1, 0.25 and 1.2 respectively, the incident angle α is supposed to be zero, the dimensionless wave number in the medium I is $k_1 a = 0.1$ (low frequency waves). The results show the DSCF continuously decreases around $0 < \theta < 5\pi/6$ and $7\pi/6 < \theta < 2\pi$ with the increasing of *s*, but the DSCF increases around $5\pi/6 < \theta < 7\pi/6$ with the increasing of *s*. The DSCF is symmetric about the angle $\theta = 0$.

Figure 5 shows the distribution of DSCF at surface parameter $s = 0, 0.1, 0.5, 1$ when k^*, μ^*, m^* equal 2, 0.25 and 1.2 respectively, the incident angle $\alpha = 0$, The dimensionless wave number in the medium I is $k_1 a = 2$ (high frequency waves). The results show the DSCF continuously decreases around $\pi/6 < \theta < 5\pi/6$ and $7\pi/6 < \theta < 5\pi/3$ with the increasing of *s*, but the DSCF increases around $-\pi/6 < \theta < \pi/6$ and $5\pi/6 < \theta < 7\pi/6$ with the increasing of *s*. The DSCF is symmetric about the angle $\theta = 0$.

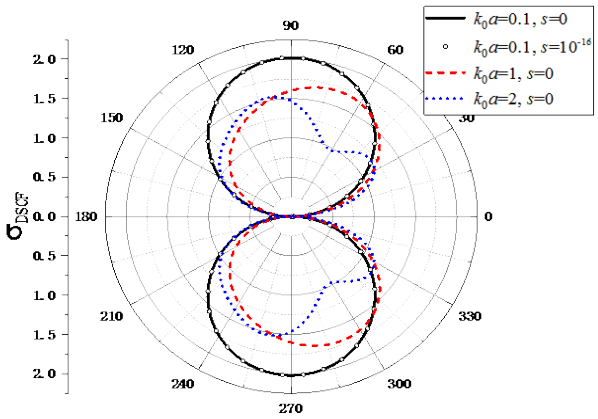

Figure 3. The verification of the present method.

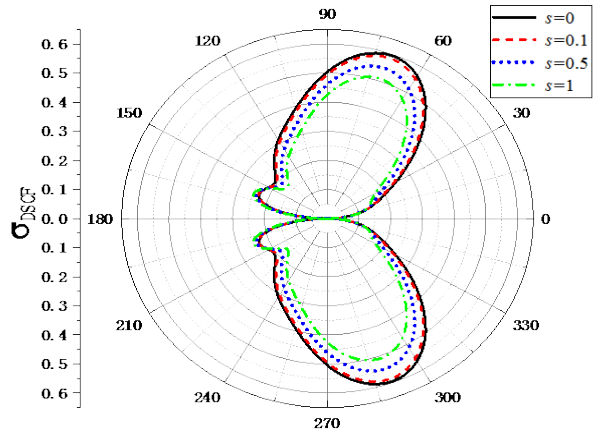

Figure 4. Distribution of DSCF with s ($k_1 a = 0.1$, $k^* = 0.1$, $\mu^* = 0.25$, $m^* = 1.2$, $\alpha = 0$).

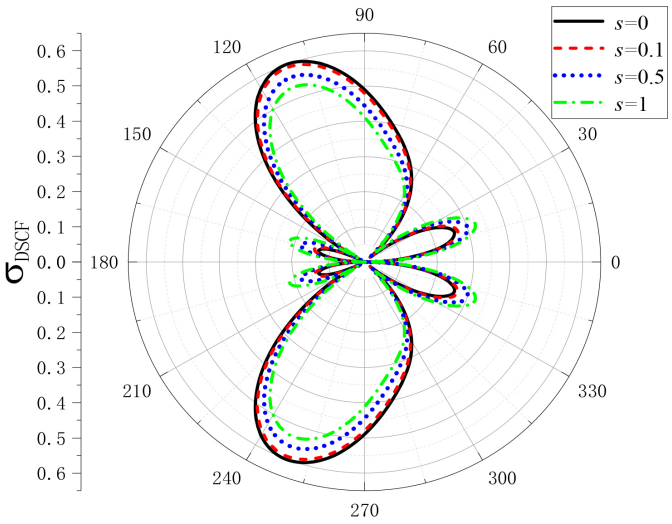

Figure 5. Distribution of DSCF with s ($k_1a=2$, $k^*=2$, $\mu^*=0.25$, $m^*=1.2$, $\alpha=0$).

Figure 6 shows the distribution of DSCF at surface parameter $s=0,0.1,0.5,1$ when k^*,μ^*,m^* equal 0.1, 4 and 1.2 respectively, the incident angle $\alpha=0$, The dimensionless wave number in the medium I is $k_1a=0.1$ (low frequency waves). The results show the DSCF continuously decreases with the increasing of *s*. The DSCF is symmetric about the angle $\theta=0$. When the medium I is softer than the inclusion (**Figure 4**), the DSCF is small, but when the medium I is harder than the inclusion (**Figure 6**), the DSCF turns bigger.

Figure 7 shows the distribution of DSCF at surface parameter $s=0,0.1,0.5,1$ when k^*,μ^*,m^* equal 0.1, 0.25 and 0.8 respectively, the incident angle $\alpha=0$, The dimensionless wave number in the medium I is $k_1a=0.1$ (low frequency waves). The results show the DSCF continuously decreases with the increasing of *s*. The DSCF is symmetric about the angle $\theta=0$. Due to $m^*=0.8<1$, the **Figure 7** is more regular Compared with **Figure 4**.

Figure 8 shows the distribution of DSCF at surface parameter $s=0,0.1,0.5,1$ when k^*,μ^*,m^* equal 0.1, 0.25 and 0.8 respectively, the incident angle $\alpha=\pi/2$, The dimensionless wave number in the medium I is $k_1a=0.1$ (low frequency waves). The results show the DSCF continuously decreases around $-5\pi/3<\theta<\pi/3$ and $2\pi/3<\theta<4\pi/3$ with the increasing of *s*, but the DSCF increases around $\pi/3<\theta<2\pi/3$ and $4\pi/3<\theta<5\pi/3$ with the increasing of *s*. The DSCF is symmetric about the angle $\theta=\pi/2$.

Figure 9 demonstrates the influence of shear modulus ratio μ^* on distribution of DSCF, the surface parameter $s=0.5$, the value of DSCF decreases with the μ^* increasing. The DSCF are symmetric distributed in the results.

Figure 10 presents the DSCF around the inclusion with different the incident angle α when the dimensionless incident wave number equals to $k_1a=0.1$ (low frequency waves). It can be found that the distributions of DSCF are very complex. These phenomena indicate that the distributions of DSCF are effected by the shape of the inclusion obviously.

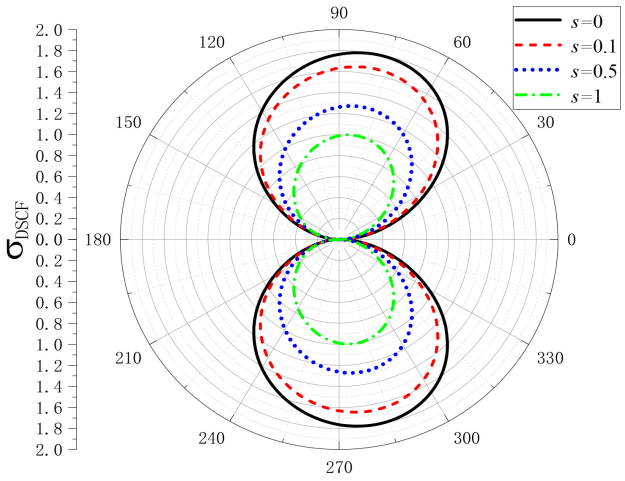

Figure 6. Distribution of DSCF with s ($k_1 a = 0.1$, $k^* = 0.1$, $\mu^* = 4$, $m^* = 1.2$, $\alpha = 0$).

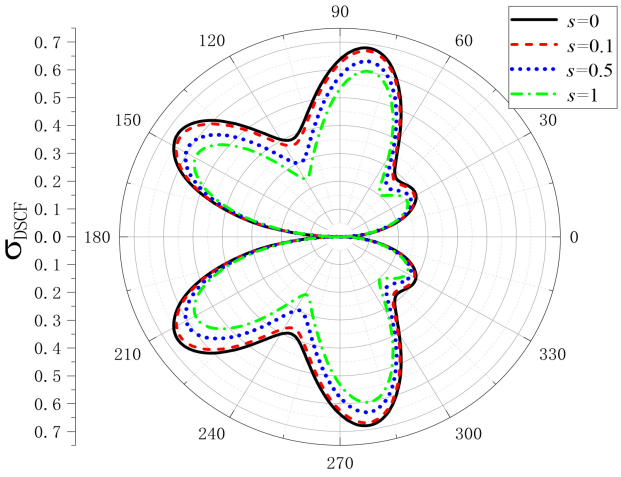

Figure 7. Distribution of DSCF with s ($k_1 a = 0.1$, $k^* = 0.1$, $\mu^* = 0.25$, $\mu^* = 0.25$, $\alpha = 0$).

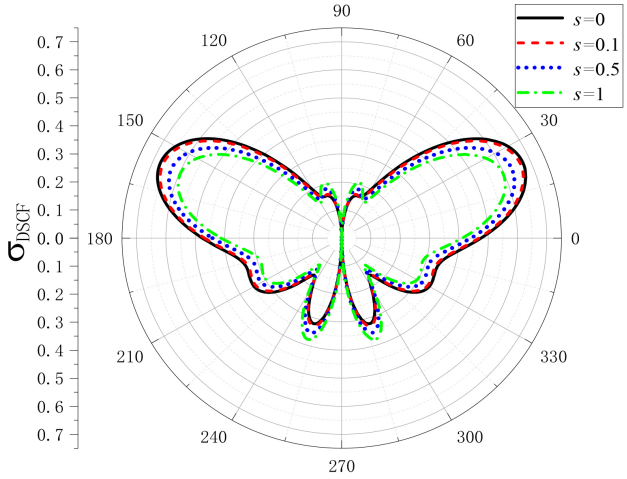

Figure 8. Distribution of DSCF with s ($k_1 a = 0.1$, $k^* = 0.1$, $\mu^* = 0.25$, $m^* = 0.8$, $\alpha = \pi/2$).

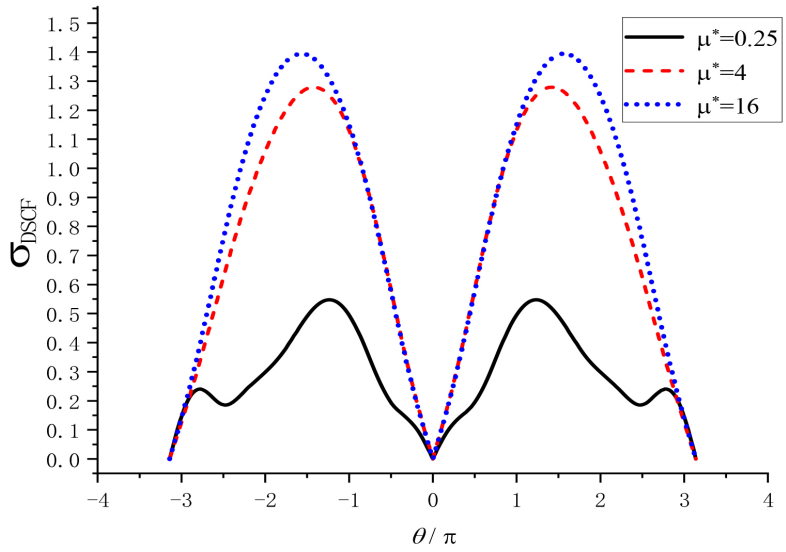

Figure 9. Distribution of DSCF with μ^* ($k_1 a = 0.1$, $k^* = 0.1$, $s = 0.5$, $m^* = 0.8$, $\alpha = 0$).

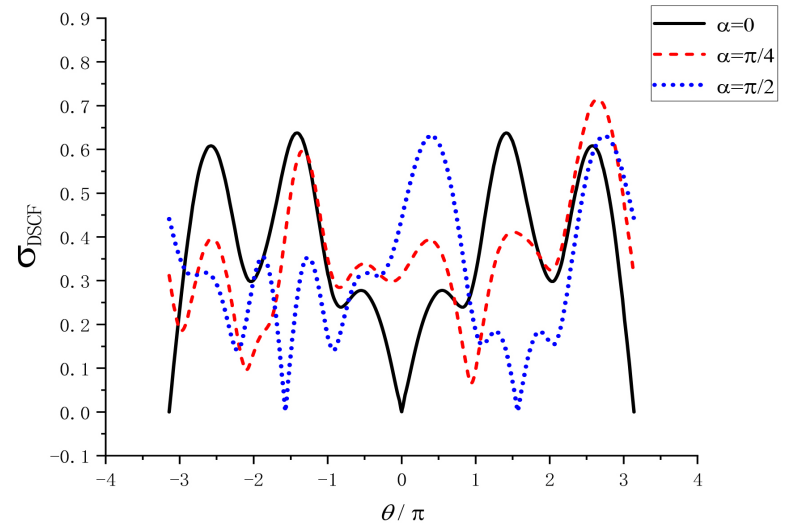

Figure 10. Distribution of DSCF with α ($k_1 a = 0.1$, $k^* = 0.1$, $s = 0.5$, $m^* = 0.8$, $\mu^* = 0$).

5. Conclusions

Based on the methods of complex function, conformal mapping, dynamic response of a nanoscale arbitrary Shape Inclusion embedded an infinite plane is analyzed. Typical results are calculated to demonstrate influences on the distribution of DSCF by principal parameters as follows:

1) As the surface parameter increases, the distribution of DSCF around the inclusion decreases.

2) The distribution of DSCF around the inclusion becomes complicated, especially under vertically incident wave.

3) The value of DSCF fluctuates with the increasing of the incident wave

number.

4) The distribution of DSCF around the inclusion increases with shear modulus ratio μ^* increases.

These results are helpful in understanding the dynamic mechanical properties of nanocomposites.

Acknowledgements

This work is supported by the Science and Technology Research Center of Xinjiang University of Science and Technology (Grant NO. 2022KYPT17).

Conflicts of Interest

The author declares no conflicts of interest regarding the publication of this paper.

References

[1] Baron, M.L. and Mattews, A.T. (1961) Diffraction of a Pressure Wave by a Cylindrical Cavity in an Elastic Medium. *Journal of Applied Mechanics*, **28**, 347-354. https://doi.org/10.1115/1.3641710

[2] Pao, Y.H. and Mow, C.C. (1973) Diffraction of Elastic Waves and Dynamic Stress Concentrations. *Journal of Applied Mechanics*, **40**, 872. https://doi.org/10.1115/1.3423178

[3] Liu, D.K. and Liu, H.W. (1998) Scattering and Dynamic Stress Concentration of SH-Wave by Interface Circular Hole. Chinese *Journal of Theoretical and Applied Mechanics*, **30**, 597-604.

[4] Davis, C.A., Lee, V.W. and Bardet, J.P. (2001) Transverse Response of Underground Cavities and Pipes to Incident SV Waves. *Earthquake Engineering & Structural Dynamics*, **30**, 383-410. https://doi.org/10.1002/eqe.14

[5] Liu, D.K., Yang, Z.L. and Liu, J.B. (2001) Scattering and Dynamic Stress Concentration of SH-Wave by Removable Rigid Cylindrical Interface Inclusion. *Journal of Harbin Engineering University of C.E. & Architecture*, **34**, 1-7.

[6] Yang, Z.L., Yan, P.L. and Liu, D.K. (2009) Scattering of SH-Waves and Ground Motion by an Elastic Cylindrical Inclusion and a Crack in Half Space. *Chinese Journal of Theoretical and Applied Mechanics*, **41**, 229-235.

[7] Chen, Z.G. (2012) Dynamic Stress Concentration around Shallow Cylindrical Cavity by SH Wave in Anisotropically Elastic Half-Space. *Rock and Soil Mechanics*, **33**, 899-905.

[8] Yang, Z.L., Hei, B.P and Yang, Q.Y. (2015) Dynamic Analysis on a Circular Inclusion in a Radially Inhomogeneous Medium. *Chinese Journal of Theoretical and Applied Mechanics*, **47**, 539-543.

[9] Sahmani, S., Bahrami, M. and Aghdam, M.M. (2015) Surface Stress Effects on the Postbuckling Behavior of Geometrically Imperfect Cylindrical Nanoshells Subjected to Combined Axial and Radial Compressions. *International Journal of Mechanical Sciences*, **100**, 1-22. https://doi.org/10.1016/j.ijmecsci.2015.06.004

[10] Miller, R.E. and Shenoy, V.B. (2000) Size-Dependent Elastic Properties of Nanosized Structural Elements. *Nanotechnology*, **11**, 139-147. https://doi.org/10.1088/0957-4484/11/3/301

[11] Dingreville, R., Qu, J. and Cherkaoui, M. (2005) Surface Free Energy and Its Effect on the Elastic Behavior of Nanosized Particles, Wires and Films. *Journal of the Mechanics and Physics of Solids*, **53**, 1827-1854. https://doi.org/10.1016/j.jmps.2005.02.012

[12] Wang, G.F. and Wang, T.J. (2006) Surface Effects on the Diffraction of Plane Compressional Waves by a Nanosized Circular Hole. *Applied Physics Letters*, **89**, Article ID: 231923. https://doi.org/10.1063/1.2403899

[13] Wang, G.F. (2006) Multiple Diffraction of Plane Compressional Waves by Two Circular Cylindrical Holes with Surface Effects. *Journal of Applied Physics*, **105**, Article ID: 013507. https://doi.org/10.1063/1.3054517

[14] Ru, Y., Wang, G.F. and Wang T.J. (2009) Diffractions of Elastic Waves and Stress Concentration Near a Cylindrical Nano-Inclusion Incorporating Surface Effect. *Vibration and Acoustics*, **131**, Article ID: 061011. https://doi.org/10.1115/1.4000479

[15] Ou, Z.Y. and Lee, D.W. (2012) Effects of Interface Energy on Scattering of Plane Elastic Wave by a Nano-Sized Coated Fiber. *Journal of Sound and Vibration*, **331**, 5623-5643. https://doi.org/10.1016/j.jsv.2012.07.023

[16] Ou, Z.Y. and Lee, D.W. (2012) Effects of Interface Energy on Multiple Scattering of Plane Compressional Waves by Two Cylindrical Fibers. *International Journal of Applied Mechanics*, **4**, Article ID: 1250040. https://doi.org/10.1142/S1758825112500408

[17] Ou, Z.Y. and Sun, Y.Q. (2019) Surface Effects on the Scatter of SH-Wave by a Shallow Buried the Elliptical Hole. *Open Journal of Applied Sciences*, **9**, 480-491. https://doi.org/10.4236/ojapps.2019.96038